Thermochimica Acta, 223 (1993) 109–120
Elsevier Science Publishers B.V., Amsterdam

Calcination kinetics of limestone and the microstructure of nascent CaO

Q. Zhong *,[1] and I. Bjerle

Department of Chemical Engineering II, Chemical Center, Lund University, S-221 00 Lund (Sweden)

(Received 23 December 1992; accepted 22 January 1993)

Abstract

The calcination kinetics of limestone was investigated by TGA at 600–1000°C and from 1 mbar to 1 atm. The temperature, total pressure, CO_2 partial pressure and particle size affect the calcination rate. Above 90% of calcination efficiency can be reached in less than 2.5 s at 1000°C and 1 mbar. Under the conditions of eliminating all diffusion resistances, the instantaneous rate of calcination is proportional to the surface area of undecomposed $CaCO_3$, and this process can be described by a shinking core model. The microstructure of nascent CaO that was prepared in an entrained-flow reactor at 1 atm, was studied using the BET method. The BET surface area of the calcines increases with increasing residence time and temperature in less than 2 s and below 1000°C. The largest BET surface area and cumulative pore volume of 2 s nascent CaO are obtained at 1000°C and 700°C, respectively.

INTRODUCTION

Furnace dry-sorbent injection is a potentially attractive retrofit technology for the reduction of SO_2 emissions from coal-fired boilers. When limestone sorbents are injected into the high-temperature regions of industrial boilers and furnaces, the sorbent is rapidly calcined to form CaO which subsequently combines with gaseous SO_2 to form calcium sulfate ($CaSO_4$). Because of the obvious difference between the molar volume of $CaCO_3$ (36.9 $cm^3\ mol^{-1}$) and CaO (16.9 $cm^3\ mol^{-1}$), the CaO formed in the calcination process is porous with a theoretical porosity of 54%. The sulfation of porous calcines with SO_2 consists of the reaction at the CaO surface, pore diffusion of SO_2 through the particle, and solid-state diffusion through the $CaSO_4$ product layer. All three of these processes are directly dependent on the microstructural properties of the nascent CaO which are

* Corresponding author.
[1] Visiting researcher from the East China Institute of Technology, 210014 Nanjing, People's Republic of China.

not the inherent properties of the parent sorbent but are a result of the thermal history during calcination [1]. Thus calcination also affects the sulfation reactivity and capacity of the calcines.

It is generally considered that the decomposition of small $CaCO_3$ particles is an instantaneous surface reaction [2–4]. Borgwardt [4] found from his entrained-flow reactor studies that 90% calcination was reached in 0.25 s for 10 μm limestone particles at 1000°C, but for differential reactor tests, it took 40 s for 90% calcination to be reached for 6 μm particles at 710°C.

The calcination kinetics affects the BET surface area and porosity of the calcines. Borgwardt [4] found that the CaO had a minimum grain size and maximum surface area immediately following $CaCO_3$ decomposition. Beruto et al. [3] calcined 3–10 μm $CaCO_3$ under vacuum at 510°C, the measured BET surface area of the calcine being 133 $m^2 g^{-1}$. Milne et al. [5] reported by SEM observation, that flash-calcined and slowly calcined sorbents were different in structure. They found that slowly calcined CaO displayed non-uniform grains which were jointed together by necks to form a continuous porous matrix, whereas the flash-calcined materials showed little internal porosity, a smaller grain size and plate-like grain shapes.

The influence of sorbent particle size and calcination atmosphere on the decomposition rate of $CaCO_3$ is also reported. The reduction of sorbent particle size can enhance the $CaCO_3$ decomposition rate [4]. Snow et al. [6] and Hajaligol et al. [7] reported that $CaCO_3$ does not decompose to CaO prior to the sulfation by controlled CO_2 partial pressure below 900°C.

The objective of this study was to investigate the calcination kinetics of limestone under vacuum conditions in TGA. The microstructure of nascent CaO prepared in an entrained-flow reactor at 1 atm was studied using the BET method.

EXPERIMENTAL

Test sorbent

Forsby limestone and Myanit dolomite were used in most of the study. A summary of the chemical and physical properties of these materials is presented in Table 1.

TGA measurements

The TGA used in the study was a Cahn-2000 electrobalance with a sample basket made of a fine Pt-net. A schematic diagram of the TGA system has been published elsewhere [8]. To prepare the sample, the basket was dipped in a slurry containing 10–15 wt.% of stone; about 5 mg of solid

TABLE 1

Chemical (wt.%) and physical properties of the samples

$CaCO_3$	$MgCO_3$	SiO_2	Al_2O_3	Fe_2O_3	MgO	K_2O	Na_2O	S	BET surface/ ($m^2\,g^{-1}$)
Limestone									
95.6	–	0.26	0.3	0.23	0.88	0.01	0.09	0.11	10.8
Dolomite									
52.5	43.9	2.9	0.3	0.4					1.5

particles adhered to the basket. The basket was then dried under IR radiation in order to form a very thin layer of sample. For all calcination experiments, the reactor system was evacuated and kept at a desired pressure in a constant gas flow of chosen proportions of N_2 and CO_2. The furnace was heated to the desired temperature, and was then moved rapidly to surround the quartz reactor. It took about 10 s for the reactor to reach temperature equilibrium with the furnace; then the calcination started. The calcination was continuously registered in the form of weight loss of the basket.

Entrained-flow reactor

An entrained-flow reactor (EFR) was used to prepare the samples for BET measurement. The EFR system consists of two main parts, a fluidized sand bed dryer and a drop-tube entrained-flow reactor. The experimental set up and operating procedure have been described elsewhere [8].

BET measurement

Both the BET surface and pore-size distribution measurements were conducted in a Cahn 2000 electrobalance-based system. In the BET method, nitrogen was used as the adsorption gas. From the adsorption/desorption isotherm, the pore size distribution can be calculated.

RESULTS AND DISCUSSION

The calcination kinetics

The calcination rate of Forsby limestone was investigated in TGA as a function of temperature, total pressure, CO_2 partial pressure and particle size, as shown in Figs. 1–5.

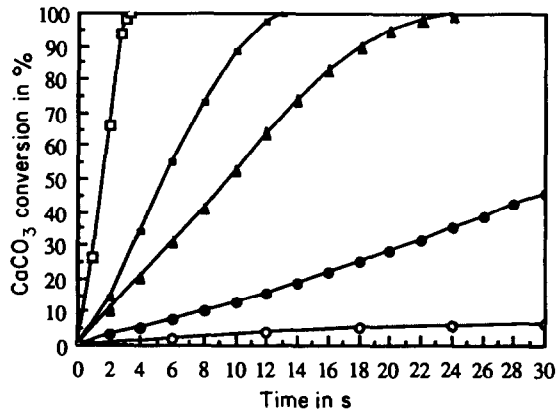

Fig. 1. The effect of reaction time and temperature on calcination efficiency for Forsby limestone at 1 mbar and 600–1000°C: ○, 600°C; ●, 700°C; ▲, 800°C; ■, 900°C; □, 1000°C.

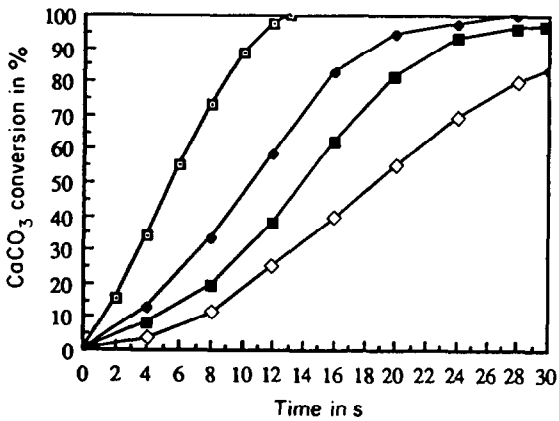

Fig. 2. The effect of total pressure on calcination efficiency for Forsby limestone at 900°C: ⊡, 1 mbar; ◆, 4 mbar; ■, 8 mbar; ◇, 1 atm.

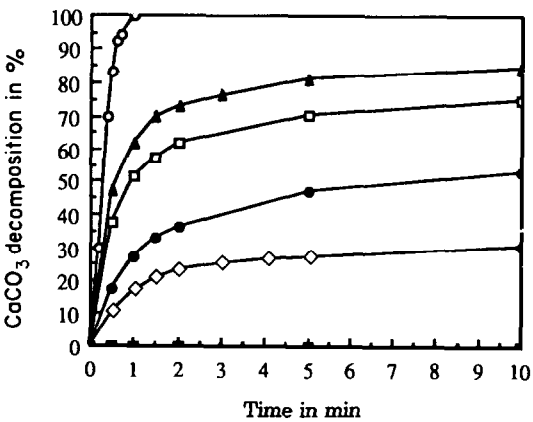

Fig. 3. The effect of CO_2 partial pressure on $CaCO_3$ decomposition rate for Forsby limestone at 900°C and a total pressure of 1 atm: ○, without CO_2; ▲, 0.1 atm CO_2; □, 0.2 atm CO_2; ●, 0.3 atm CO_2; ◇, 0.4 atm CO_2; ■, 0.5 atm CO_2.

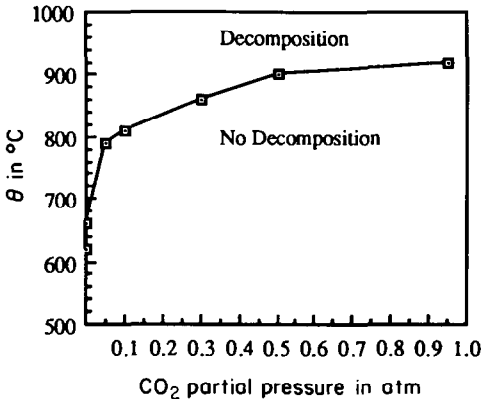

Fig. 4. The effect of CO_2 partial pressure on $CaCO_3$ decomposition temperature for Forsby limestone at 900°C and 1 atm.

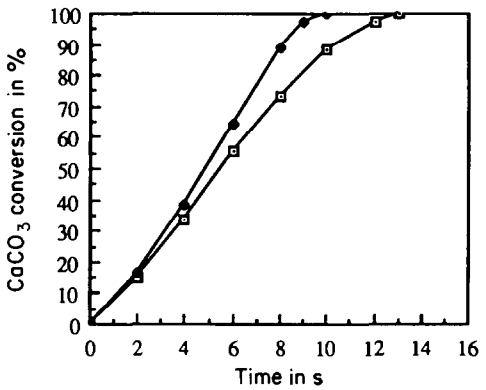

Fig. 5. The effect of particle size on calcination efficiency for Forsby limestone at 900°C and 1 mbar: ⊡, unground; ◆, ground for 7 h.

Temperature

Figure 1 shows that the overall rate of calcination is strongly influenced by temperature in the region 600–1000°C and at 1 mbar total pressure. The rate increases rapidly with increasing temperature. The calcination rate is rather slow at 600°C. When the temperature is 1000°C, more than 90% calcination efficiency can be reached in less then 2.5 s.

Total pressure

The effect of total pressure on calcination rate is shown in Fig. 2. The effect of total pressure is obvious, and is similar to that found by Steen et al. [9]. The calcination of $CaCO_3$ consits of the decomposition of $CaCO_3$ at the CaO–$CaCO_3$ interface, diffusion of CO_2 through the CaO product layer, and diffusion of CO_2 through the gas fllm at the particle surface. The latter

two processes are directly related to the total pressure of the gas phase. The diffusion resistances of CO_2 through the CaO layer and the gas fllm increase with increasing total pressure, thus the overall rate of calcination decreases.

CO_2 partial pressure

The effect of CO_2 partial pressure on the calcination rate of $CaCO_3$ was investigated at 900°C and 1 atm, as shown in Fig. 3. The decomposition of $CaCO_3$ clearly decreases with increasing CO_2 partial pressure. When CO_2 partial pressure is above 0.5 atm, the material does not decompose. These phenomena may be interpreted in terms of the basic thermodynamics of the $CaCO_3$–CaO–CO_2 system. For the reversible reaction

$$CaCO_3(s) \underset{r_b,k_b}{\overset{-r_a,k_a}{\rightleftharpoons}} CaO(s) + CO_2(g) \tag{1}$$

where k_a is a decomposition rate constant (kmol m^{-3} s^{-1} atm^{-1}) and k_b a composition rate constant (kmol m^{-3} s^{-1} atm^{-1}). The decomposition rate of $CaCO_3$ ($-r_a$/(kmol m^{-3} s^{-1})) and the composition rate of $CaCO_3$ (r_b/(kmol m^{-3} s^{-1})) may be expressed as

$$-r_a = k_a p_{CaCO_3} \tag{2}$$

$$r_b = k_b p_{CaO} p_{CO_2} \tag{3}$$

where p_{CaCO_3} and p_{CaO} are the partial pressures of $CaCO_3$ and CaO, respectively. So

$$\frac{-r_a}{r_b} = K_p \frac{1}{p_{CO_2}} \tag{4}$$

where

$$K_p = \frac{k_a}{k_b} \frac{p_{CaCO_3}}{p_{CaO}}$$

Because the partial pressure of the solid phase is constant, the equilibrium constant K_p (atm) is a function of temperature alone. At a given temperature, therefore, increasing the CO_2 partial pressure leads to a decrease in the rate ratio. This means that the decomposition rate of $CaCO_3$ decreases with increasing partial pressure of CO_2 and the composition rate of $CaCO_3$ increases. When the CO_2 partial pressure exceeds its equilibrium partial pressure ($p^*_{CO_2}$), $CaCO_3$ cannot decompose. Figure 4 shows the decomposition temperature versus CO_2 equilibrium partial pressure at 1 atm. Up to 650°C in a gas stream of N_2, Forsby limestone does not decompose. Under 810°C, 10% CO_2 concentration in the gas phase is sufficient to prevent decomposition. For the 95% CO_2 mixture, the decomposition temperature is about 920°C. Similar results have been reported by Snow et al. [6] and Hajaligol et al. [7].

Particle size

Figure 5 shows that the calcination rate of ground sample is faster than that of unground sample, because ground samples have smaller diffusion resistances of CO_2 through the CaO layer and gas film, and have a larger BET surface area.

Calcination model

Calcination model

According to the above results, it is clear that the overall rate of calcination is dependent on the temperature, total pressure of the gas phase, CO_2 concentration and particle size. Sitcox et al. [10] developed a mathematical model of calcination that includes decomposition of $CaCO_3$ at the CaO–$CaCO_3$ interface, diffusion of CO_2 through the CaO layer and gas film, and continuous surface area loss. This model is mathematically complex and requires a lot of parameters that at present are not available.

Under the conditions of eliminating diffusion resistances of CO_2 through the CaO layer and gas film, the instantaneous rate of calcination is proportional to the surface area of the undecomposed $CaCO_3$ (A_{CaCO_3} in m^2) [4, 5]. It is

$$\frac{dn_{CaCO_3}}{dt} = -k_c A_{CaCO_3} \tag{5}$$

where n_{CaCO_3} is the undecomposed $CaCO_3$ in the sample (kmol) and k_c is a rate constant (kmol m^{-2} s^{-1}). It is assumed that the calcination process can be described by a shinking-core model. Thus for a spherical particle

$$X_{CaCO_3} = 1 - \left(\frac{d_c}{d_p}\right)^3$$

where X_{CaCO_3} is the conversion of $CaCO_3$, and d_p and d_c are the diameters of the initial and undecomposed $CaCO_3$ particles, respectively. Integration of eqn. (5) yields

$$\frac{1-(1-X_{CaCO_3})^{1/3}}{t} = \frac{2k'}{d_p} \tag{6}$$

where k' ($=k_c/\rho_p$) is a reaction rate constant (m s^{-1}) and ρ_p is the $CaCO_3$ density (27 kmol m^{-3}).

For a flat-plate sample geometry

$$X_{CaCO_3} = 1 - \frac{L}{L_0}$$

where L_0 and L are the layer thickness of the initial and undecomposed $CaCO_3$ samples, respectively. Integrating eqn. (5), we obtain

$$X_{CaCO_3} = \frac{k'}{L_0} t \tag{7}$$

Model prediction

In the TGA system, the sample is coated on the Pt basket and forms a layer that is very thin compared to the wire diameter; thus, the sample geometry could be considered as being a plate [11]. Under the experimental conditions of 1 mbar total pressure and 5 mg sample, the diffusion resistances of CO_2 through the CaO layer and gas film can be eliminated. Figure 6 shows the comparison of the experimental data and calcination model predictions (using eqn. (7)) for Forsby limestone at 1 mbar and 600–1000°C. The rate constant (k') is obtained by fitting the model calculations to experimental data. An Arrhenius plot has been made, as shown in Fig. 7. The reaction activation energy from the slope of the straight line is estimated as 110.63 kJ mol^{-1}.

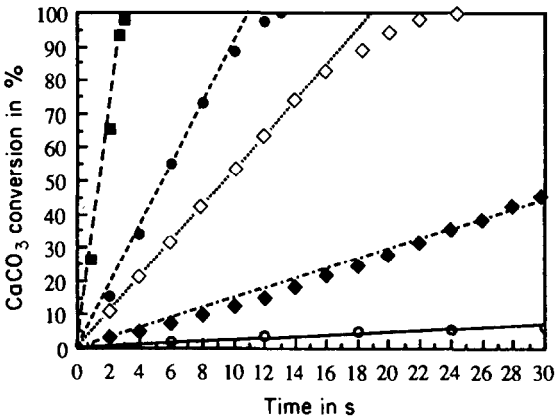

Fig. 6. Model predictions of the influence of reaction time and temperature compared to experimental data for Forsby limestone at 1 mbar and 600–1000°C: ○, 600°C, exp.; ——, 600°C, model; ◆, 700°C, exp.; –·–·–·, 700°C, model; ◊, 800°C, exp.; · · ·, 800°C, model; ●, 900°C, exp.; – – –, 900°C, model; ■, 1000°C, exp.; — — —, 1000°C, model.

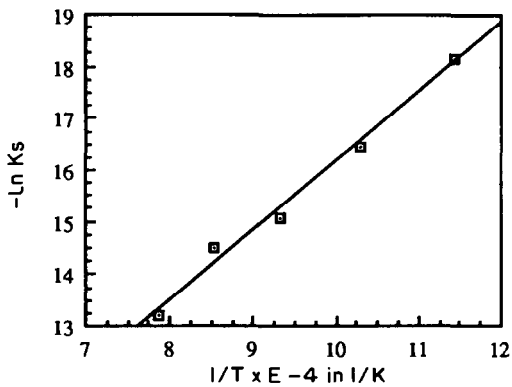

Fig. 7. Arrhenius plot for evaluation of reaction activation energy for Forsby limestone at 1 mbar and 600–900°C.

Nascent CaO microstructure

Samples for BET measurement were prepared in the entrained-flow reactor at 1 atm. The calcined Forsby limestone and Myanit dolomite were found to exhibit type-IV adsorption isotherms according to the BDDT classification [12], as shown in Fig. 8. Type IV isotherms are characteristic of materials with porosity in the mesopore range, and typically exhibit a hysteresis loop. The hysteresis loops for the calcined Forsby and Myanit samples have shapes corresponding to a type-B hysteresis, which is associated with slit-shaped pores or spaces between parallel plates [13].

The effects of residence time and particle size on the microstructure of nascent CaO were investigated for the Forsby and Myanit samples in the absence of SO_2, as shown in Fig. 9. These figures indicate that the BET surface areas of nascent CaO increase with increasing residence time.

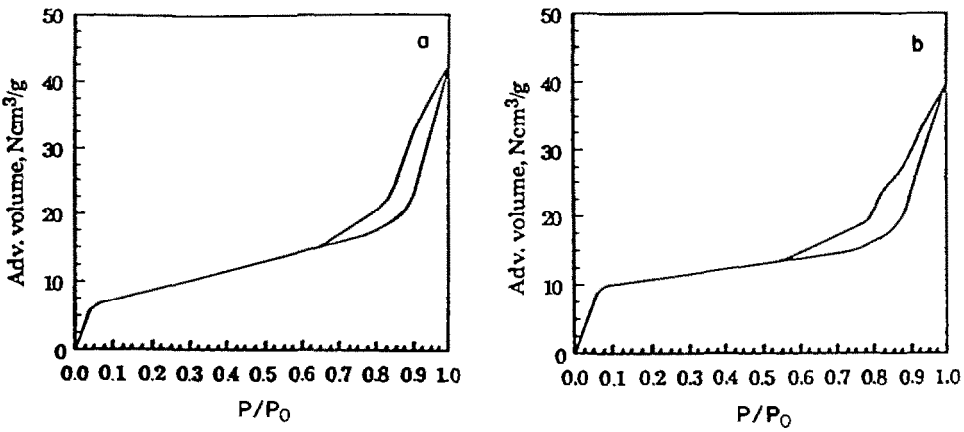

Fig. 8. Nitrogen adsorption/desorption isotherms. a, Forsby limestone; b, Myanit dolomite.

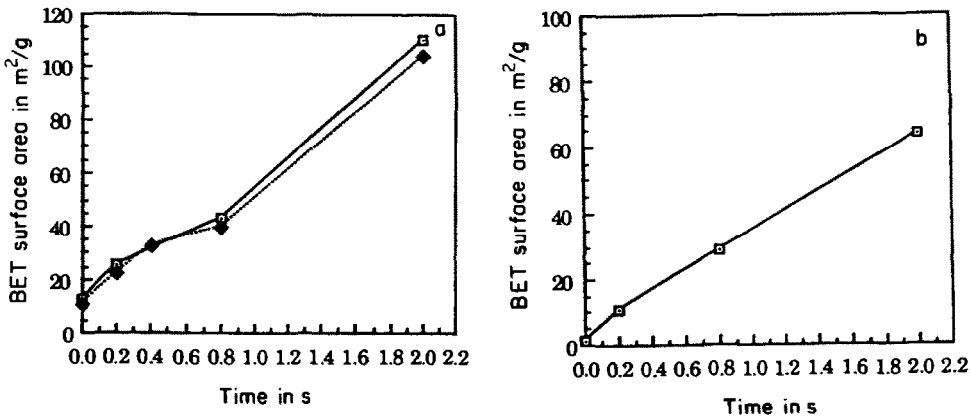

Fig. 9. Influence of residence time and particle size on BET surface area after calcination at 1000°C. a, Forsby limestone: ◆, unground; ⊡, ground for 7 h. b, Myanit dolomite, unground.

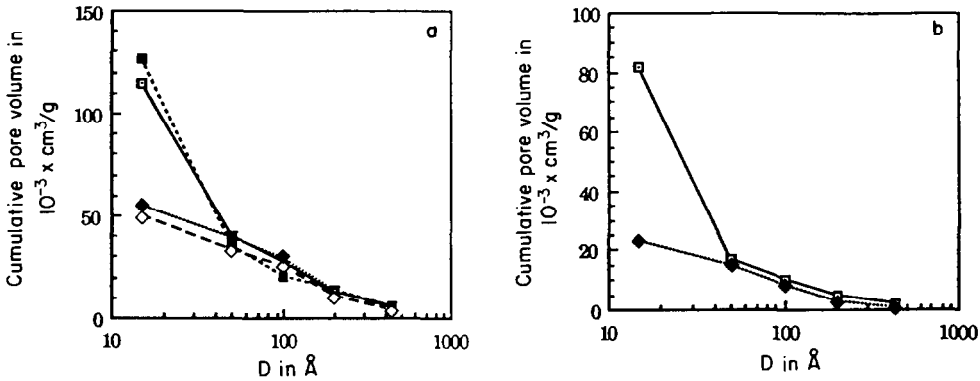

Fig. 10. Pore size distribution after calcination at 1000°C for 0.2 s and 2 s. a, Forsby limestone: ⊡, 2 s, 7 h ground; ◆, 0.2 s, 7 h ground; ■, 2 s, unground; ◇, 0.2 s, unground. b, Myanit dolomite: ⊡, 2 s, unground; ◆, 0.2 s, unground.

Newton et al. [14] found in their entrained-flow reactor that the surface areas of calcined sorbent did not vary significantly over the residence time range of 0.05–0.4 s. From Fig. 10, it is obvious that 0.2 s nascent CaO has almost the same cumulative pore volume as 2 s nascent CaO, the pore diameter being larger than 50 Å. Figure 10a also shows that the BET surface area of calcines after grinding is larger than for unground samples. In Fig. 11, the pore size distribution for the Myanit and Forsby samples are compared on a weight basis and it is obvious that the pore volume of Myanit dolomite is smaller than that of Forsby limestone.

The BET surface area and pore structure of nascent calcium oxide are strongly affected by the calcination temperature. Figure 12 shows that the BET surface area increases with rising calcination temperature below 1000°C. Above 1000°C sintering starts to take place. When the reaction temperature exceeds 1100°C, the sintering is significant. The largest BET

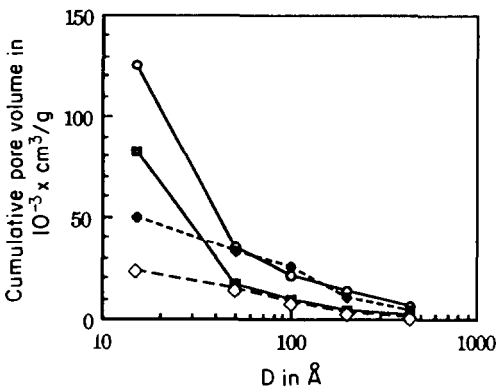

Fig. 11. Pore size distribution for Forsby limestone and Myanit dolomite after calcination at 1000°C, 0.2 s and 2 s residence time: ○, Forsby 2 s; ◆, Forsby 0.2 s; ■, Myanit 2 s; ◇, Myanit 0.2 s.

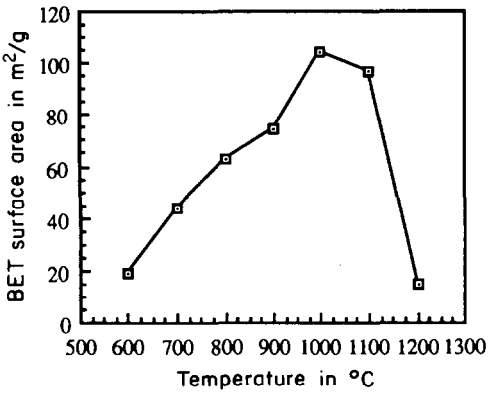

Fig. 12. The effect of temperature on BET surface area for Forsby limestone after 2 s calcination.

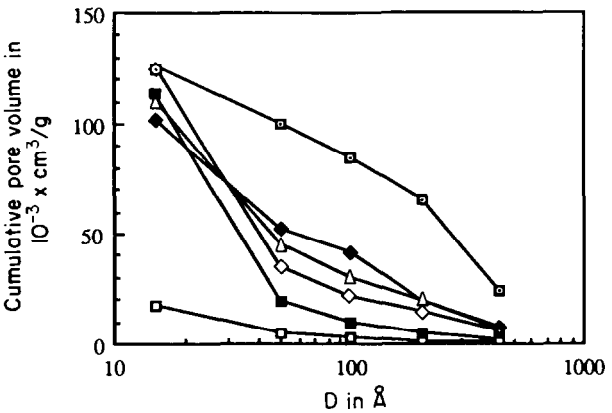

Fig. 13. Pore size distribution after calcination at 700–1200°C and 2 s residence time: ⊡, 700°C; ◆, 800°C; △, 900°C; ◇, 1000°C; ■, 1100°C; □, 1200°C.

surface area is obtained at 1000°C. High temperature accelerates the calcination, but at the same time, causes sintering to take place. Figure 13 shows the pore structure change with increasing calcination temperature. The largest cumulative pore volume is obtained at 700°C while the smallest is found at 1200°C. The shift of the size distribution to larger pores is not observed during the sintering. This is similar to the effect observed by Dogu [15].

CONCLUSIONS

The calcination of $CaCO_3$ is a complex process which includes $CaCO_3$ decomposition at the CaO–$CaCO_3$ interface, and diffusion of CO_2 through the CaO product layer and the gas film. Temperature, total pressure, CO_2 partial pressure and particle size affect the calcination rate. Above 90% of calcination efficiency can be reached in less than 2.5 s in TGA at 1000°C and

1 mbar. Under the conditions of eliminating all diffusion resistances, the instantaneous rate of calcination is proportional to the surface area of undecomposed $CaCO_3$, and this process can be described by a shrinking core model.

The calcination kinetics affects the BET surface area and porosity of nascent CaO. The BET surface area of the calcines increases with increasing residence time and temperature in less than 2 s and below 1000°C. The largest BET surface area and cumulative pore volume of 2 s nascent CaO are obtained at 1000°C and 700°C, respectively.

REFERENCES

1 L.J. Muzio and G.R. Offen, J. Air Pollut. Control. Assoc., 37 (1987) 642.
2 E.P. Hyatt, I.B. Cutler and M.E. Wadsworth, J. Am. Ceram. Soc., 41 (1985) 70.
3 D. Beruto, L. Barco, A.W. Searcy and G. Spinolo, J. Am. Ceram. Soc., 63 (1980) 439.
4 R.H. Borgwardt, AIChE J., 31 (1985) 103.
5 C.R. Milne, G.D. Silcox and D.W. Pershing, Ind. Eng. Chem. Res., 29 (1990) 139.
6 M.J. Snow, J.P. Longwell and A.F. Sarofim, Ind. Eng. Chem. Res., 27 (1988) 268–273.
7 M.R. Hajaligol, J.P. Longwell and A.F. Sarofirm, Ind. Eng. Chem. Res., 27 (1988) 2203–2210.
8 I. Bjerle, F. Xu and Z. Ye, Chem. Eng. Technol., 15 (1992) 151–161.
9 H. Steen, K. Li and H. Roga, Environ. Sci. Technol., 14 (1980) 588–593.
10 G.D. Sitcox, J.C. Kramlich and D.W. Pershing, Ind. Eng. Chem. Res., 28 (1989) 155–160.
11 F. Xu, I. Bjerle, A. Karlsson and S. Kiuru, Dry injection–experimental studies using TGA technique, in Proc. ACHEMASIA'89, International Meeting on Chemical Engineering and Biotechnology, 1st Exhibition Congress, Oct. 1989, Beijing, PRC.
12 S.J. Gregg and K.S.W. Sing, Adsorption, Surface Area and Porosity, Academic Press, London, 2nd edn., 1982.
13 S. Lowell and J.E. Shields, Powder Surface Area and Porosity, Chapman and Hall, London, 2nd edn., 1984.
14 G.H. Newton, S.L. Chen and J.G. Kramlich, AIChE J., 35 (1989) 988.
15 T. Dogu, Chem. Eng. J., 21 (1981) 213.